Neurobiology of Disease

Elevated Galectin-3 Is Associated with Aging, Multiple Sclerosis, and Oxidized Phosphatidylcholine-Induced Neurodegeneration

Sara Xue,[1*] Brian M. Lozinski,[1*] Samira Ghorbani,[1] Khanh Ta,[2] Charlotte D'Mello,[1] V. Wee Yong,[1] and Yifei Dong[2]

[1]Hotchkiss Brain Institute and the Department of Clinical Neuroscience, University of Calgary, Calgary, Alberta T2N 4N1, Canada and [2]Department of Biochemistry, Microbiology, and Immunology, College of Medicine, University of Saskatchewan, Saskatoon, Saskatchewan S7N 5E5, Canada

Aging is a significant risk factor associated with the progression of CNS neurodegenerative diseases including multiple sclerosis (MS). Microglia, the resident macrophages of the CNS parenchyma, are a major population of immune cells that accumulate in MS lesions. While they normally regulate tissue homeostasis and facilitate the clearance of neurotoxic molecules including oxidized phosphatidylcholines (OxPCs), their transcriptome and neuroprotective functions are reprogrammed by aging. Thus, determining the factors that instigate aging associated microglia dysfunction can lead to new insights for promoting CNS repair and for halting MS disease progression. Through single-cell RNA sequencing (scRNAseq), we identified *Lgals3*, which encodes for galectin-3 (Gal3), as an age upregulated gene by microglia responding to OxPC. Consistently, excess Gal3 accumulated in OxPC and lysolecithin-induced focal spinal cord white matter (SCWM) lesions of middle-aged mice compared with young mice. Gal3 was also elevated in mouse experimental autoimmune encephalomyelitis (EAE) lesions and more importantly in MS brain lesions from two male and one female individuals. While Gal3 delivery alone into the mouse spinal cord did not induce damage, its co-delivery with OxPC increased cleaved caspase 3 and IL-1β within white matter lesions and exacerbated OxPC-induced injury. Conversely, OxPC-mediated neurodegeneration was reduced in Gal3$^{-/-}$ mice compared with Gal3$^{+/+}$ mice. Thus, Gal3 is associated with increased neuroinflammation and neurodegeneration and its overexpression by microglia/macrophages may be detrimental for lesions within the aging CNS.

Key words: **aging; galectin 3; microglia; multiple sclerosis; neurodegeneration; oxidized phosphatidylcholine**

Significance Statement

Aging accelerates the progression of neurodegenerative diseases such as multiple sclerosis (MS). Understanding the molecular mechanisms of aging that increases the susceptibility of the CNS to damage could lead to new strategies to manage MS progression. Here, we highlight that microglia/macrophage-associated galectin-3 (Gal3) was upregulated with age exacerbated neurodegeneration in the mouse spinal cord white matter (SCWM) and in MS lesions. More importantly, co-injection of Gal3 with oxidized phosphatidylcholines (OxPCs), which are neurotoxic lipids found in MS lesions, caused greater neurodegeneration compared with injection of OxPC alone, whereas genetic loss of Gal3 reduced OxPC damage. These results demonstrate that Gal3 overexpression is detrimental to CNS lesions and suggest its deposition in MS lesions may contribute to neurodegeneration.

Received Dec. 19, 2022; revised Apr. 25, 2023; accepted May 5, 2023.

Author contributions: V.W.Y. and Y.D. designed research; S.X., B.M.L., S.G., K.T., C.D., and Y.D. performed research; S.X., B.M.L., and Y.D. analyzed data; S.X. and Y.D. wrote the first draft of the paper; B.M.L., S.G., C.D., V.W.Y., and Y.D. edited the paper; Y.D. wrote the paper.

This work was supported by the Multiple Sclerosis Society of Canada (MSSOC) Grant 3527 and the Canadian Institutes of Health Research (CIHR) Grant FDN 167270 (to V.W.Y.) and Startup Funding from the University of Saskatchewan (Y.D.). S.X. had studentship support from the Alberta Multiple Sclerosis Network and Alberta Innovates. Y.D. had postdoctoral fellowship support from CIHR. S.G. had postdoctoral fellowship support from the Harley N. Hotchkiss Postdoctoral Fellowship and CIHR. B.M.L. had studentships from the Alberta Graduate Excellence Scholarship and MSSOC. V.W.Y. received salary support from the Canada Research Chair (Tier 1) Program. We thank the Hotchkiss Brain Institute Advanced Microscopy Platform facility for microscopy and image analysis platforms and the Centre for Health Genomics and Informatics for sequencing.

*S.X. and B.M.L. contributed equally to this work.

The authors declare no competing financial interests.

Correspondence should be addressed to Yifei Dong at jeff.dong@usask.ca or V. Wee Yong at vyong@ucalgary.ca.

https://doi.org/10.1523/JNEUROSCI.2312-22.2023

Introduction

Aging is a natural process that increases the risk and progression of neurodegenerative diseases such as multiple sclerosis (MS), where pain and disability impact longevity and the quality of life (Hou et al., 2019). Determining what mediates age-related processes that accelerate neurodegeneration and disease progression will provide critical insights for managing and treating MS. Microglia are long-lived, self-renewing tissue resident macrophages found in the parenchyma of the CNS (Dong and Yong, 2019). They regulate CNS homeostasis and perform important custodial functions including tissue surveillance (Madry et al., 2018), synaptic remodeling (Parkhurst et al., 2013), and cell debris clearance (Diaz-Aparicio et al., 2020). Microglia also rapidly respond to insults (Davalos et al., 2005), and they accumulate in large numbers at sites of damage such as within active lesions or around the border of slowly-expanding and chronic active lesions found in the brains of people with MS (Zrzavy et al., 2017; Jäckle et al., 2020; Yong and Yong, 2022).

While microglia normally clear debris to limit damage in the CNS (Mandrekar et al., 2009; Lampron et al., 2015; Keren-Shaul et al., 2017; Bellver-Landete et al., 2019; Herzog et al., 2019; Cignarella et al., 2020; Willis et al., 2020; Dong et al., 2021b; Ennerfelt et al., 2022), their neuroprotective functions may be impaired by aging. Single-cell RNA sequencing (scRNAseq) studies demonstrate aging microglia have significantly altered transcriptomes (Hammond et al., 2019; Olah et al., 2020; Safaiyan et al., 2021; Dong et al., 2022). Functionally, aging microglia are more proinflammatory (von Leden et al., 2017; Michaels et al., 2020; Kaya et al., 2022), less motile (Damani et al., 2011; Hefendehl et al., 2014), and fail to properly neutralize lipids and cell debris during injury (Cantuti-Castelvetri et al., 2018; Rawji et al., 2018; Dong et al., 2022). Since these results demonstrate microglia dysfunction contributes to a worse disease outcome in the aging CNS, investigating what causes these impairments could lead to new treatments for age associated progression of neurodegeneration in MS.

We recently found that aging exacerbates neurodegeneration in the mouse spinal cord white matter (SCWM) after stereotactic injection of oxidized phosphatidylcholines (OxPCs; Dong et al., 2022), which is a neurotoxic lipid peroxidation product found in MS and other neurologic diseases (Haider et al., 2011; Dong et al., 2021b; Muñoz et al., 2022; Zrzavy et al., 2021). Using scRNAseq and spatial RNAseq, we also compared microglia transcriptomic changes in response to aging and OxPC-mediated neurodegeneration, and we found *Lgals3* overexpression by aging microglia from OxPC lesions (Dong et al., 2022). *Lgals3* encodes for galectin-3 (Gal3), a β-galactoside-binding lectin which is associated with microglia activation, neurodegeneration, and CNS vascular injury (Barake et al., 2020; Puigdellívol et al., 2020; Mehina et al., 2021; Tan et al., 2021; Boza-Serrano et al., 2022). Indeed, microglia-secreted Gal3 may act as an endogenous toll-like receptor 4 (TLR) ligand (Burguillos et al., 2015) whereas Gal3 deficiency reduces neuroinflammation (Jiang et al., 2009) and increases neuron survival (Margeta et al., 2022) in mice. These studies highlight a detrimental role for Gal3 accumulation in the CNS during disease and suggest Gal3 overexpression by aging microglia may increase CNS tissue's susceptibility to inflammation and injury. However, data to support the detrimental role for Gal3 remain sparse.

In this study, we aimed to investigate the relationship between Gal3 and neuroinflammation or neurodegeneration in the CNS by comparing its expression in young (six weeks) and middle-aged (52 weeks) mice with focal SCWM lesions or with experimental autoimmune encephalomyelitis (EAE) lesions, as well as in postmortem MS lesions. We also provide new evidence that Gal3 increases neuroinflammation and neurodegeneration in response to OxPC deposition. Since OxPC accumulate in MS and other neurologic diseases (Dong and Yong, 2022) and cause worse damage in the aging CNS (Dong et al., 2022), these results suggest therapeutically targeting Gal3 may attenuate OxPC-mediated injuries and help to slow the progression of neurodegeneration in diseases such as MS.

Materials and Methods

MS specimens

Frozen brain tissue from postmortem patients with secondary progressive MS were obtained from the Multiple Sclerosis and Parkinson's Tissue Bank located at Imperial College, London (www.ukmstissuebank.imperial.ac.uk). The brain lesions stained for this project originated from two males (45 and 43 years old), and one female (42 years old). The use of the MS specimens is approved by The Conjoint Health Research Ethics Board at the University of Calgary.

Mice

All experiments were conducted with ethics approval (protocol number AC21-0154 and AC21-0174) from the Animal Care Committee at the University of Calgary under regulations of the Canadian Council of Animal Care. Female six- and 52-week-old C57Bl/6J mice were acquired from The Jackson Laboratory for *in vivo* experiments assessing Gal3 in aging OxPC and lysophosphatidylcholine (LPC) SCWM lesions, whereas 10- to 12-week-old mice were used for EAE experiments. Female C57Bl/6 mice six- to eight-week-old from Charles River were used for the OxPC and Gal3 co-injection experiments. Eight- to 10-week-old female C57Bl/6 ($Gal3^{+/+}$) and B6.Cg-$Lgals3^{tm1Poi/J}$ ($Gal3^{-/-}$) mice from The Jackson Laboratory were used to compare OxPC lesions with or without Gal3 expression. Mice were maintained on a regular diet in low humidity environment on a 12/12 h light/dark cycle at 21–23°C with unlimited access to food and water. Mice and littermates were randomly assigned to different experimental groups.

Spinal cord surgery

The surgical procedure for stereotactic spinal cord injection was performed as described from previous studies (Dong et al., 2021a, b, 2022). Briefly, six- and 52-week-old mice were anesthetized and injected with 5 µg of 1-palmitoyl-2-azelaoyl-sn-glycero-3-phosphocholine (PAzePC; Sigma), or with 1% LPC (Sigma), resuspended in 0.5-µl sterile PBS at 10 mg/ml into the ventral SCWM between the T3 and T4 vertebra. PBS alone was injected as the sham control. $Gal3^{+/+}$ and $Gal3^{-/-}$ mice were injected with 1 µg PAzePC in PBS using the same procedure. Alternatively, 1 µg PAzePC, 500 ng of mouse recombinant Gal3 (Biolegend), or 1 µg PAzePC and 500 ng of Gal3 in PBS were injected for experiments determining the effect of excess Gal3 in the SCWM using the same procedure. After the injection, the needle was left in place for 2 min to prevent back flow, and then the mouse was sutured and placed in a thermally controlled environment for recovery.

Spinal cord isolation and processing

As described previously (Dong et al., 2021a, b, 2022), spinal cords were isolated from mice euthanized 3 or 7 d after OxPC, Gal3, or OxPC and Gal3 injections, or after 7 or 14 d following LPC injection. After overnight fixation in 4% paraformaldehyde at 4°C, tissues were dehydrated in 30% sucrose solution for at least 48 h and frozen in FSC22 Frozen Section Media (Leica). The spinal cord tissue was then cut coronally into 20-µm sections using a cryostat (Thermo Fisher Scientific), collected on to Superfrost Plus microscope slides (VWR), and stored at −20°C before staining and analysis.

Experimental autoimmune encephalomyelitis (EAE)

Ten- to 12-week-old C57Bl/6 female mice (The Jackson Laboratory) were subcutaneously injected with 50 μg per 100 μl myelin oligodendrocyte

glycoprotein (MOG) 35–55 peptide (Protein and Nucleic Acid Facility, Stanford University School of Medicine) in complete Freund's adjuvant supplemented with 4 mg/ml heat-inactivated Mycobacterium tuberculosis H37Ra (Sigma-Aldrich). A total of 50-μl emulsion was deposited on either side of the tail base. Pertussis toxin (300 ng per 200 μl; 180, List Biological Laboratories) was intraperitoneally injected on days 0 and 2 after MOG immunization. Daily monitoring of EAE mice was performed, and the mice were scored on a scale of 0–15. EAE mice during peak disease (days 16–18) were euthanized and spinal cords were dissected and as stated above for the spinal cord injections. Alternatively, EAE was induced in young (eight-week) and aging (52-week) female C57BL/6 wild-type mice (The Jackson Laboratory). Spinal cord tissues were dissected from EAE mice 12 d after onset of clinical signs with average EAE score of 7.8 (young) versus 7.6 (aging) of a 15-point scale. Mice were euthanized with ketamine (100 mg/kg) and xylazine (10 mg/kg) injected intraperitoneally and then perfused with PBS through the left ventricle of the heart. Following PBS perfusion, thoracic spinal cord was dissected for immunohistochemistry.

Primary mouse neuron culture

Primary mouse cortical neurons from embryonic day 15–16 pups were isolated and grown in Neurobasal Plus media (Invitrogen) with B27 Plus supplement (Invitrogen) as detailed (Cua et al., 2013; Dong et al., 2021a). Neurons were stimulated with or without 10 μg/ml of Gal3 for 24 h. Four replicate wells were used per experimental condition. After 24 h, cells were fixed with 4% PFA for 10 min, permeabilized with 0.2% Triton X-100 in PBS for 10 min, blocked with Odyssey blocking buffer (LI-COR) for 45 min, labeled with primary antibodies overnight at 4°, washed once with PBS, then labeled with secondary antibodies and DAPI at 1 μg/ml for 30 min, washed once with PBS, and resuspended in 100 μl of PBS for quantitative fluorescence microscopy analysis.

Antibodies

The following primary antibodies were used for immunofluorescence microscopy: chicken anti-mouse glial fibrillary acidic protein (GFAP; clone SMI24, 1:1000 dilution, Biolegend), mouse anti-Gal3 (clone A3A12, 1:200 dilution, Abcam), rat anti-Gal3 (clone eBioM3/38, 1:200 dilution, Thermo Fisher Scientific), rat anti-mouse/human CD45 (clone 30-F11, 1:500 dilution, Thermo Fisher Scientific), rabbit anti-human/mouse IBA1 (catalog #019-19741, 1:1000 dilution, Fujifilm Wako), rat anti-mouse CD16/32 (clone 2.4G2, 1:1000 dilution, BD Pharmigen), goat anti-mouse/human IBA1 (catalog #PA5-18039, 1:1000 dilution, Thermo Fisher Scientific), rabbit anti-mouse neurofilament heavy chain (NFH, catalog #RPCA-NF-H, 1:1000 dilution, Encor Biotechnology), chicken anti-mouse neurofilament heavy chain (catalog #CPCA-NF-H, 1:2000 dilution, Encor Biotechnology), rat anti-mouse myelin basic protein (MBP; clone 12, 1:500 dilution, Abcam), goat anti-mouse IL-1β (catalog #AF-401, 1:40, R&D Systems), rat anti-mouse-induced nitric oxide synthase (iNOS, clone CXNFT, 1:200, Invitrogen), rabbit anti-mouse arginase 1 (Arg1, clone D3E3M, 1:200, Cell Signaling Technology), goat anti-mouse oligodendrocyte transcription factor 2 (OLIG2, catalog #AF2418, 1:1000, R&D Systems), rabbit anti-mouse cleaved caspase-3 (clone Asp175, 1:200, Cell Signaling Technology), mouse anti-Tubulin β3 (TUJ1, clone Tuj1, 1:500, Biolegend), rabbit anti-amyloid-β precursor protein (βAPP, catalog #36-6900, 1:200, Thermo Fisher Scientific).

The following secondary antibodies from Jackson ImmunoResearch were used at 1:400 dilution: Alexa Fluor 488 donkey anti-mouse IgG, cyanine Cy3 donkey anti-chicken IgY, Alexa Fluor 647 donkey anti-rat IgG, cyanine Cy3 donkey anti-rat IgG, Alexa Fluor 488 donkey anti-goat IgG, Alexa Fluor 647 donkey anti-rabbit IgG.

Mouse spinal cord histology

Spinal cords sections were stained with eriochrome cyanine (EC; 10% $FeCl_3$) and neutral red (NR, 1%) to visualize demyelinated spinal cord lesions as described in previous studies (Dong et al., 2021b, 2022). Brightfield images were then acquired with 10 × 0.4 NA air objective using the Olympus VS110 Slidescanner. Region of interest (ROI) containing SCWM lesions were selected using demyelinated areas that have lower EC staining and higher NR staining in the ventral SCWM and their areas were quantified using the CEllSens Dimension software (Olympus). Total spinal cord lesion volume was estimated by multiplying the sum of all lesion ROIs in serial spinal cord sections from each sample by the distance separating each serial section (400 μm).

Labeling tissues for immunofluorescence confocal microscopy

Microscope slides containing mouse spinal cord samples were processed for confocal microscopy as previously described (Dong et al., 2021b, 2022). Briefly, slides were warmed to room temperature (RT) for 10 min. For myelin basic protein (MBP) labeling, slides were first delipidated by successive wash of 50%, 70%, 90%, 95%, 100%, 95%, 90%, 70%, and 50% ethanol. Slides were then rehydrated in PBS (10 min), permeabilized with 0.2% Triton X-100 in PBS (10 min), and blocked with horse blocking solution (PBS, 10% horse serum, 1% BSA, 0.1% cold fish stain gelation, 0.1% Triton X-100, 0.05% Tween 20) for 1 h at RT. Samples were then incubated overnight with primary antibodies in antibody dilution buffer (PBS, 1% BSA, 0.1% cold fish stain gelation, 0.1% Triton X-100) at 4°C. The next day, slides were then washed thrice with 0.2% Tween 20 in PBS (5 min each), and then incubated with secondary antibodies and 1 μg/ml of DAPI resuspended in the antibody dilution buffer for 1 h at RT. The slides were washed thrice more as above, and coverslips were mounted onto the slides using Fluoromount-G solution (SouthernBiotech).

For postmortem MS tissue samples, after slides were warmed to RT, they were fixed with 4% paraformaldehyde for 10 min, then washed in PBS for 10 min to remove excess PFA. The remaining steps were the same as mouse spinal cord samples stated.

Confocal microscopy

Laser confocal immunofluorescence images were acquired using the Leica TCS Sp8 laser confocal microscope at RT, using the 25 × 0.95 NA water objective. The 405-, 488-, 552-, and 640-nm lasers were used to excite the fluorophores from antibodies bound to samples and detected by two low dark current Hamamatsu PMT detectors and two high sensitivity hybrid detectors. Images were acquired in 8-bits, in a z-stack using unidirectional scanning, 1 airy unit pinhole, 0.75× zoom, and 0.57-μm optical sections and 2048 × 2048 pixels *xy* resolution. Alternatively, images were acquired using the Zeiss LSM700 confocal microscope with a 20 × 0.8 NA air objective using similar settings. Equal laser, gain, and offset settings to maximize contrast and minimize saturation were consistently used for all samples within experiment sets. A sample slide stained with only the secondary antibodies and DAPI was used for each experiment to control for nonspecific secondary immunofluorescence. Leica Application Suite X or Zeiss Zen (black edition) was used for image acquisition, ImageJ was used for image threshold and particle analysis.

Confocal image analysis

Z-stack confocal images of spinal cords were analyzed with ImageJ (Fiji, NIH) as in previous study (Dong et al., 2021b, 2022). For each channel/marker z-stack, maximum intensity projections were created and converted from eight-bit to RGB. The lesion ROI or equivalent area in PBS sham controls or the contralateral normal appear white matter (NAWM) was drawn. The area outside the ROI was not analyzed. Positive signal was determined using the color brightness threshold set consistently using a predetermined value by comparing the secondary antibody-stained control and PBS sham controls. ROI for lesions were drawn based on CD16/32, IBA1, MBP, or other lesion associated markers in the SCWM. The analyze particles function was used to create a mask to quantify the positive signals in each ROI. The threshold values for setting the positive signal, as well as the size and circularity settings for particle analysis, were used consistently across all samples for each experimental set to avoid bias. For representative images shown, maximum intensity projection of each channel/marker in a z-stack were merged and displayed using pseudo colors in ImageJ. Only brightness and contrast settings were adjusted, and consistently between samples for better displaying the images.

Quantitative fluorescence microscopy analysis

Primary mouse neurons cultured in 96-well flat bottom black/clear plates were imaged using the 10×/0.5 NA air objective on the

ImageXpress Micro XLS High-Content Analysis System (Molecular Devices). DAPI excitation 387/11 – emission 447/60 and FITC excitation 482/35 – emission 536/40 filter sets were used for image acquisition. For each well, 12 field of views (FOVs) were acquired neuron survival quantitation by multiwavelength cell scoring analysis using the MetaXpress High-Content Image Acquisition and Analysis Software (Molecular Devices). The number of $DAPI^+$ $Tuj1^+$ neurons in each sample was divided by the mean of the control samples to give the fold change value, which were plotted for statistical analysis. For representative images shown, DAPI and TUJ1 channels for the sample were merged and displayed in pseudo colors using ImageJ. Only brightness and contrast settings were adjusted, and consistently between samples for better displaying the images.

Lgals3 analysis using scRNAseq datasets

Previously generated scRNAseq datasets as detailed in (Dong et al., 2022; Dong and Yong, 2022) were analyzed using Seurat v3 in R and R studio (Butler et al., 2018) to compare *Lgals3* expression between six- and 52-week mice injected with PBS or PAzePC. Specifically, *Lgals3* expression was assessed in a previously generated Seurat object containing subsets of microglia, border-associated macrophages (BAMs), and dendritic cells (DCs)/monocytes. The FeaturePlot and VlnPlot functions were used to generate plots visualizing *Lgals3* expression in cell clusters or sample groups.

Experimental design and statistical analysis

Data were collated in Microsoft Excel and graphs were generated in GraphPad Prism 9.2. Data shown are the individual data points where each point on a graph represents a separate mouse, as well as mean ± SD. Sample size for experiments was determined based on previously published results (Dong et al., 2021b, 2022), the cost of experiment, the feasibility of the experiment, as well as the availability of sex (females) and age (six and 52 weeks) matched mice. One aging LPC sample was omitted because of imaging error, otherwise, no data were excluded from experimental analyses. Sample sizes are reported in the figure legends and only one measurement is recorded per sample. Littermate mice were randomly selected for each experimental condition and treatment. Blinding was not conducted. Quantification was performed consistently using equal settings for all samples. One-way ANOVA with Tukey's multiple comparison test was used to analyze statistically significant differences between the means of two or more treatment groups against the control group. For data with only two groups, significance was determined by Welch's unequal variances *t* test. As stated in the figure legends, asterisks indicate significance where $^*p < 0.05$, $^{**}p < 0.01$, $^{***}p < 0.001$. All experimental data are available on reasonable request.

Data availability

ScRNASeq datasets used in this paper are available to download from the NCBI Sequence Read Archive (SRA) with BioProject accession numbers: PRJNA648663 and PRJNA734097.

Results

Aging microglia overexpress *Lgals3* in response to OxPC-mediated neurodegeneration

We previously used scRNAseq to analyze microglia isolated from six- or 52-week mice stereotactically injected with PBS (sham) or PAzePC (a purified OxPC) and determined their transcriptomic changes in response to aging and/or OxPC deposition after 7 d (Dong et al., 2022). Notably, *Lgals3* was a top aging-upregulated gene in mononuclear phagocytes isolated from 52-week mice with OxPC lesions in the SCWM compared with cells from OxPC lesions in six-week mice (Fig. 1*A*). By comparing differential gene expression in cells from the four experimental groups, we identified clusters of steady-state, OxPC lesion associated, or proliferating microglia, as well as border-associated macrophages (BAMs), and dendritic cells (DCs)/monocyte (Fig. 1*B*). While BAM and DC/monocyte clusters had similar *Lgals3* expression regardless of age or OxPC lesion, *Lgal3* expression and aging associated *Lgals3* upregulation was mostly found in lesion associated and proliferating microglia but not in steady-state microglia (Fig. 1*C*,*D*). These observations are consistent with recent studies (Krasemann et al., 2017; Hammond et al., 2019; Pluvinage et al., 2019; Plemel et al., 2020; Safaiyan et al., 2021; Boza-Serrano et al., 2022; Margeta et al., 2022), albeit not emphasized in these reports, of a close association of *Lgals3* expression by microglia with neuroinflammation and neurodegeneration (Fig. 1*E*).

Aging promotes greater Gal3 accumulation in focal SCWM lesions

To determine whether aging induced elevation of *Lgals3* translated into excess Gal3 protein accumulation, we first compared between OxPC SCWM lesions of six- and 52-week mice. PAzePC was stereotactically injected into the SCWM of six- and 52-week mice and spinal cord tissue sections were analyzed after 3 and 7 d. EC and NR histologic analysis showed significantly greater OxPC lesion expansion (Welch's *t* test, $t = 2.84$, $p = 0.0293$) in the SCWM of 52-week mice compared with six-week mice after 7 d (Fig. 2*A*–*C*). We then used Gal3 specific antibodies (Extended Data Fig. 2-1) and immunofluorescence confocal microscopy to compare Gal3 expression between the SCWM lesions and the contralateral NAWM of six- and 52-week mice. While Gal3 immunofluorescence was minimal in the NAWM of six- and 52-week mice, it was significantly increased in the 52-week lesion compared with the six-week lesion at both day 3 (one-way ANOVA, $F = 4.658$, $p = 0.0297$ 52-week NAWM vs 52-week lesion, $p = 0.0342$ six-week lesion vs 52-week lesion) and day 7 (one-way ANOVA, $F = 14.32$, $p < 0.0001$ 52-week NAWM vs 52-week lesion, $p = 0.0022$ six-week lesion vs 52-week lesion) after OxPC injection (Fig. 2*D*,*F*,*H*,*J*). And although there were less $CD16/32^+$ microglia/macrophages in 52-week lesion at day 3 (one-way ANOVA, $F = 43.52$, $p < 0.0001$ six-week NAWM vs six-week lesion, $p < 0.0001$ 52-week NAWM vs 52-week lesion, $p = 0.0003$ six-week lesion vs 52-week lesion) and day 7 (one-way ANOVA, $F = 38.32$, $p < 0.0001$ six-week NAWM vs six-week lesion, $p = 0.0002$ 52-week NAWM vs 52-week lesion, $p = 0.0066$ six-week lesion vs 52-week lesion), a majority of these cells (Welch's *t* test, $t = 6.332$ and $p = 0.0006$ for day 3, $t = 4.126$ and $p = 0.0073$ for day 7) associated with Gal3 immunoreactivity (Fig. 2*D*,*E*,*G*–*I*,*K*).

We also compared Gal3 levels between six- and 52-week mice in the LPC-induced focal SCWM lesion, a model for demyelination and remyelination in MS (Plemel et al., 2018). At 7 d following stereotactic LPC injection, there was a similar age-associated significant increase in Gal3 immunoreactivity (one-way ANOVA, $F = 9.720$, $p = 0.0012$ 52-week NAWM vs 52-week lesion, $p = 0.0020$ six-week lesion vs 52-week lesion) in areas where $CD16/32^+$ microglia/macrophage accumulated within the SCWM lesions (Fig. 3*A*,*B*). Similarly, day 14 LPC lesions in 52-week mice also had significantly greater (Welch's *t* test, $t = 3.386$, $p = 0.0040$) Gal3 immunoreactivity compared with lesions from six-week mice (Fig. 3*C*,*D*). Thus, aging increases Gal3 deposition in OxPC and LPC-induced focal SCWM lesions.

Gal3 alone does not promote inflammation or injury in the CNS

To investigate whether Gal3 overexpression may impact CNS homeostasis, we first treated primary mouse neurons with or without Gal3. Neuronal survival was assessed by quantitative immunofluorescence microscopy analysis and Gal3 did not induce any loss of $TUJ1^+$ neurons after 24 h in culture (Fig. 4*A*,*B*). We

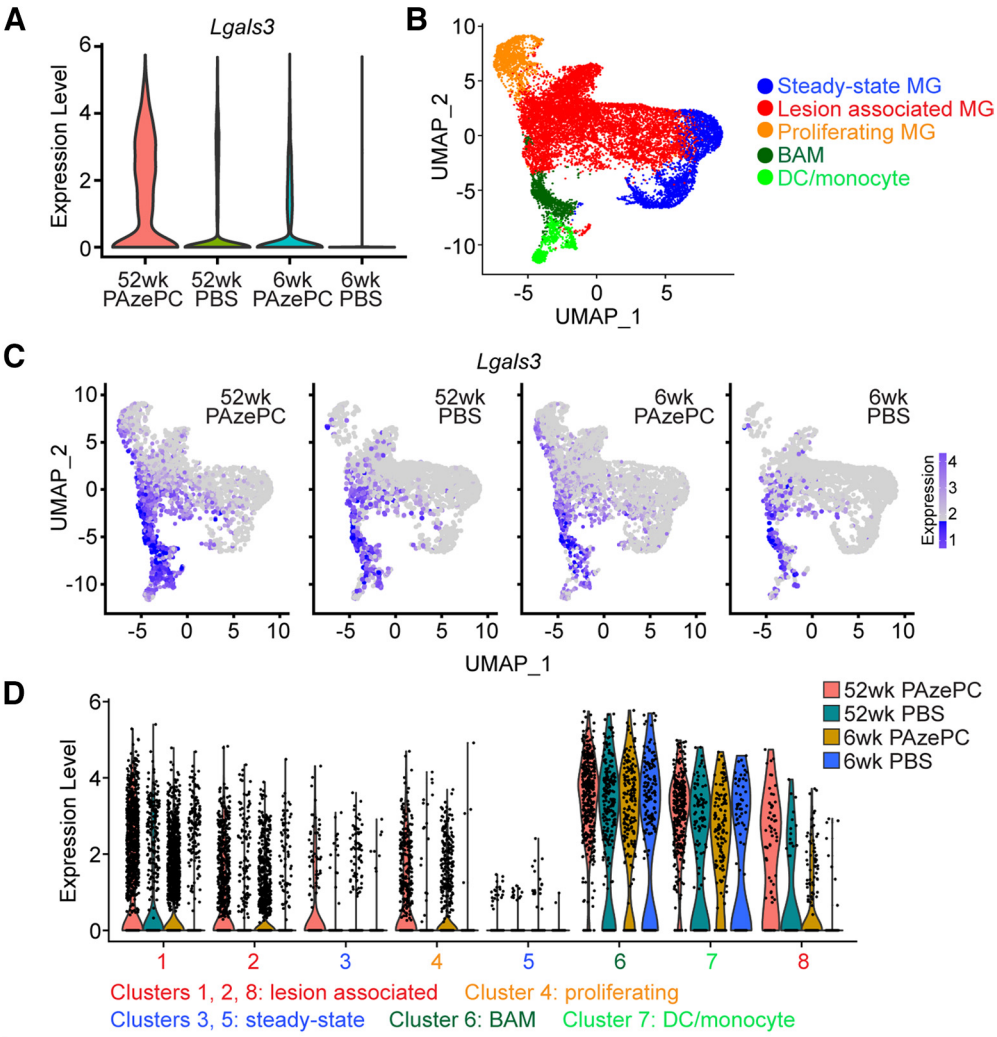

E

Context	Expression	Reference
Disease associated microglia	+	Krasemann et al., 2017
Microglia in human AD	+	Boza-Serrano et al., 2019
Aging microglia	+	Hammond et al., 2019
Aging and AD microglia	+	Pluvinage et al., 2019
Microglia in LPC injury	+	Plemel et al., 2020
Aging white matter microglia	+	Safaiyan et al., 2021
Glaucoma associated microglia	+	Margeta et al., 2022

Figure 1. *Lgals3* is upregulated in microglia during disease and aging. ***A***, Violin plot of scRNAseq comparing *Lgals3* mRNA expression in microglia isolated from the spinal cords of six- and 52-week mice 7 d after injection with PBS (sham control) or PAzePC (purified OxPC). ***B***, Annotated UMAP showing grouped clusters of steady-state (blue), OxPC lesion associated (red), and proliferating (orange) microglia, as well as border-associated macrophage (BAM; dark green) and DC/monocyte (light green). ***C***, ***D***, Feature maps (***C***) and violin plot (***D***) comparing the distribution and levels of *Lgals3* expression between different cell clusters and between experimental groups. For scRNAseq, the sample size was $n = 3$ per experimental group (each n represents a pool of 4 spinal cords for a total of 12 mice per group). ***E***, Table summarizing recent studies that report microglia Gal3 upregulation during disease and aging.

also injected PBS or mouse recombinant Gal3 into the SCWM of mice. Three days following injection, the SCWM of PBS and Gal3-injected mice appeared similar (Fig. 4*C*). Gal3 also did not cause any accumulation of IBA1$^+$ microglia/macrophages (Fig. 4*D*) nor any reactivity from GFAP$^+$ astrocytes (Fig. 4*E*). Thus, increasing Gal3 in the context of the healthy CNS did not promote neurotoxicity or inflammation.

Excess Gal3 exacerbates OxPC-mediated neuroinflammation and neurodegeneration

Since aging microglia overexpressed Gal3 in response to OxPC-mediated neurodegeneration in the SCWM (Figs. 1, 2), and Gal3 is associated with microglia reactivity and CNS damage (Jiang et al., 2009; Burguillos et al., 2015; Krasemann et al., 2017; Hammond et al., 2019; Pluvinage et al., 2019; Plemel et al., 2020; Mehina et al., 2021; Safaiyan et al., 2021; Boza-Serrano et al., 2022; Margeta et al., 2022), excessive Gal3 deposition in the CNS may contribute to aging-associated exacerbation of OxPC-mediated neurodegeneration (Dong et al., 2022). To test this hypothesis, we injected either PAzePC alone or PAzePC + Gal3 into the SCWM of mice. Using confocal microscopy analysis, we found Gal3 did not change the accumulation of IBA1$^+$ microglia/macrophage to PAzePC lesions and it did not alter the amount of Arg1 in the lesions (Fig. 5*A*,*G*,*I*). However, there was a trend of increased iNOS and significantly increased total IL-1β (Welch's

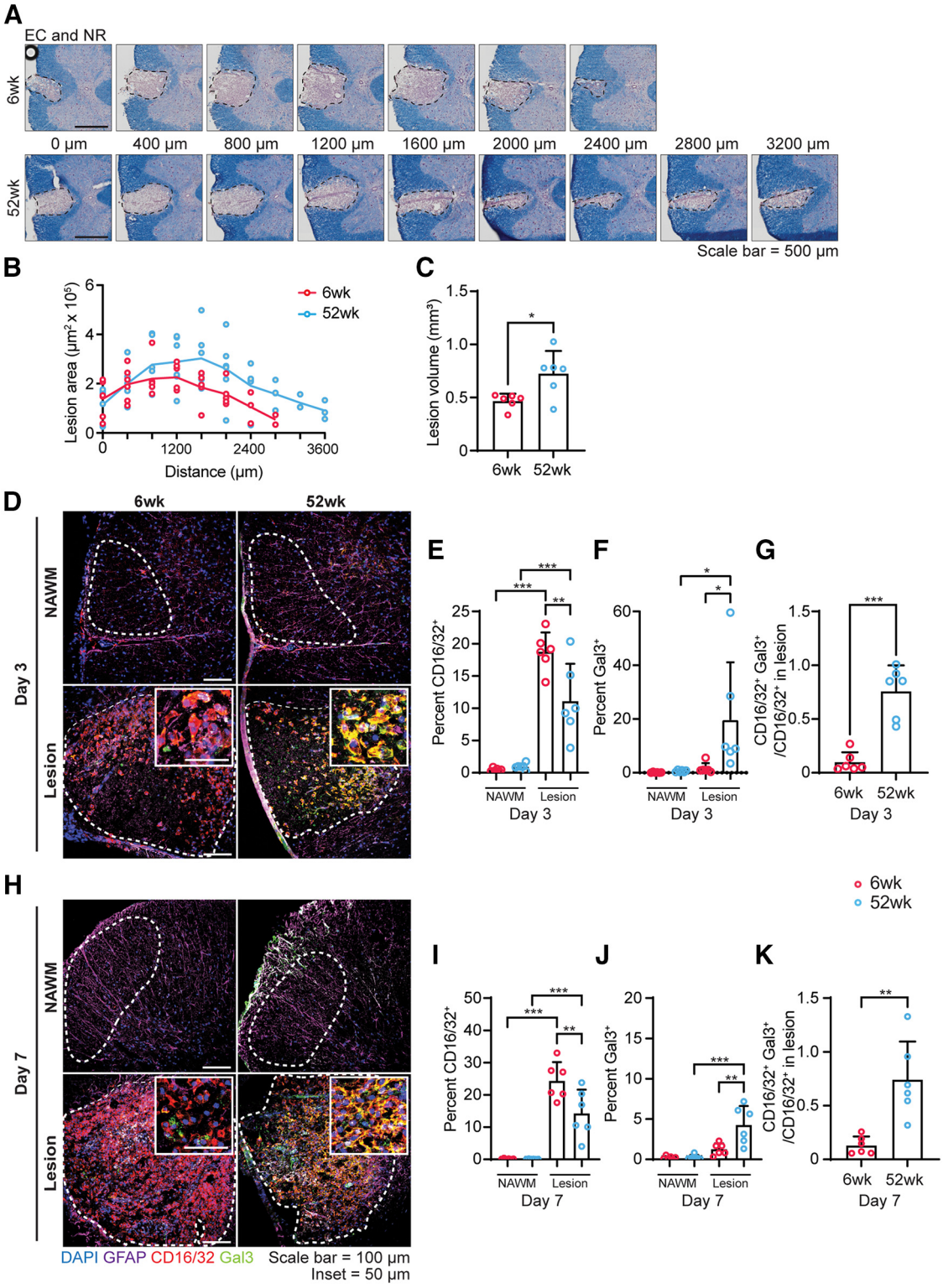

Figure 2. Gal3 is elevated in OxPC lesions of aging mice and is associated with aging microglia/macrophages. ***A***, Representative eriochrome cyanine (EC) and neutral red (NR) labeling of serial spinal cord sections from six- and 52-week mice 7 d after PAzePC injection. Black dashed lines indicate the ROI used for quantitative analyses. ***B***, ***C***, Graphs comparing day 7 spinal cord lesion spread (***B***) and total lesion volume (***C***) between six- and 52-week mice. ***D***, Representative confocal immunofluorescence images of six- and 52-week SCWM lesions or the contralateral NAWM labeled with DAPI (blue), GFAP (magenta), Gal3 (green), and CD16/32 (red) 3 d after PAzePC injection. White dashed lines indicate the ROI used for quantitative analyses. ***E–G***, Graphs comparing the percent of lesion or NAWM ROI that is CD16/32$^+$ (***E***), Gal3$^+$ (***F***), and CD16/32$^+$ Gal3$^+$ over CD16/32$^+$ proportions (***G***) three days after PAzePC injection. ***H***, Representative confocal images of six- and 52-week SCWM lesion or NAWM labeled with DAPI, GFAP, Gal3, and CD16/32 7 d after PAzePC injection. ***I–K***, Graphs comparing the percent of lesion or NAWM ROI that is CD16/32$^+$ (***I***), Gal3$^+$ (***J***), and CD16/32$^+$ Gal3$^+$ over CD16/32$^+$ proportions (***K***) 7 d after PAzePC injection. Data were acquired from two separate experiments, sample size $n = 6$ per experimental group. Significance indicated as $^*p < 0.05$, $^{**}p < 0.01$, $^{***}p < 0.001$. One-way ANOVA with Tukey's multiple comparison was used for ***E***, ***F***, ***I***, ***J***; Welch's unequal variances *t* test was used for ***C***, ***G***, ***K***. Data are represented as mean ± SD. Data are represented as mean ± SD. See Extended Data Figure 2-1.

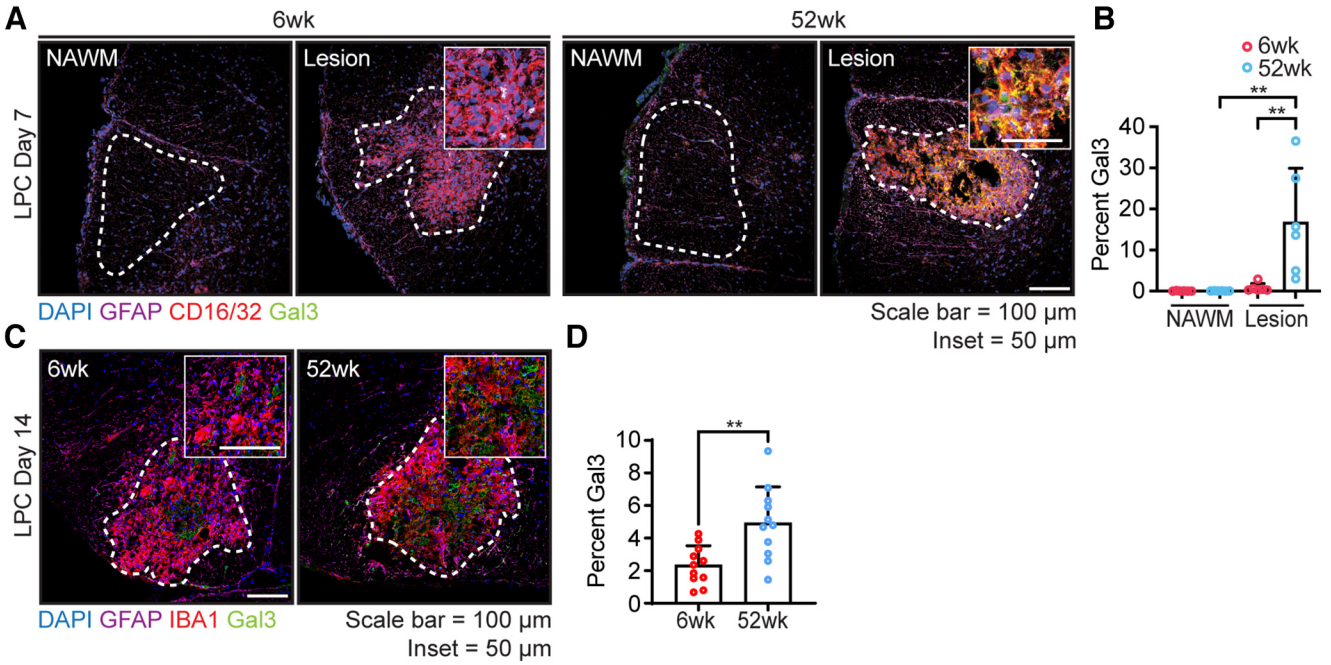

Figure 3. Gal3 is upregulated in aging LPC lesions. ***A***, Representative confocal images of six- and 52-week LPC SCWM lesions or the contralateral NAWM labeled with DAPI (blue), GFAP (magenta), Gal3 (green), and CD16/32 (red) 7 d after LPC injection. White dashed lines indicate the ROI of lesion used for quantitative analyses. ***B***, Graph comparing the percent of lesion or NAWM ROI that is Gal3$^+$ 7 d after LPC injection. Data were acquired from two separate experiments, sample size $n = 6$ per experimental group. ***C***, Representative confocal images of six- and 52-week LPC SCWM lesions labeled with DAPI (blue), GFAP (magenta), Gal3 (green), and IBA1 (red) 14 d after LPC injection. ***D***, Graph comparing the percent of lesion ROI that is Gal3$^+$ 7 d after LPC injection. Data were acquired from three separate experiments, sample size $n = 11$ per experimental group. Data are represented as mean ± SD. One-way ANOVA with Tukey's multiple comparison was used for ***B***, Welch's unequal variances *t* test was used for ***D***.

t test, $t = 3.843$, $p = 0.0027$) in the PAzePC + Gal3 lesions compared with PAzePC alone lesions (Fig. 5*A*,*B*,*H*,*J*). In addition, while the amount of myelin disruption measured by MBP, IBA1$^+$ microglia/macrophage accumulation, NFH$^+$ axon density, and OLIG2$^+$ cells were similar between PAzePC alone and PAzePC + Gal3 lesion epicenters (Fig. 5*C*,*D*,*K*–*M*), the latter contained significantly greater immunoreactivity (Welch's *t* test, $t = 3.034$, $p = 0.0135$) for cleaved caspase 3 and had a significantly greater density (Welch's *t* test, $t = 3.813$, $p = 0.0033$) of cleaved caspase 3$^+$ TUJ1$^+$ axons (Fig. 5*D*–*E*,*N*–*P*), a marker of cell death (Namura et al., 1998). Moreover, PAzePC + Gal3 lesions had significantly higher amounts (Welch's *t* test, $t = 2.692$, $p = 0.0364$) of βAPP accumulation. βAPP also significantly (Welch's *t* test, $t = 3.969$, $p = 0.0089$) overlapped with CD16/32$^+$ microglia/macrophages in PazePC + Gal3 lesions compared with PazePC alone lesions (Fig. 5*F*,*Q*–*S*). More importantly, EC and NR histologic analyses of the PAzePC alone and the PAzePC + Gal3 lesions found Gal3 promoted significantly greater (Welch's *t* test, $t = 2.545$, $p = 0.0316$) OxPC lesion volume (Fig. 6*A*–*C*). Unlike at the lesion epicenter, the proportional change of NFH$^+$ axon density between PAzePC alone or PAzePC + Gal3 lesions and their respective contralateral NAWM along the entire volume of the lesion suggested PAzePC + Gal3 induced a greater extent of axon loss compared with PAzePC alone (Fig. 6*D*,*E*). Thus, excess Gal3 increased neuroinflammation during OxPC injury and more importantly exacerbated OxPC-induced neurodegeneration.

Gal3 deficiency ameliorates OxPC-mediated damage

We next performed a loss-of-function experiment by comparing how wild-type and Gal3 deficient mice (Fig. 7*A*) responded to OxPC. Seven days after PazePC injection, spinal cords from Gal3$^{-/-}$ mice had less lesion spread and significantly reduced total lesion volume (Welch's *t* test, $t = 4.703$, $p = 0.0004$) compared with Gal3$^{+/+}$ mice (Fig. 7*B*,*C*). In addition, the Gal3$^{-/-}$ lesion epicenters were significantly smaller (Welch's *t* test, $t = 3.238$, $p = 0.0060$) and contained significantly greater density (Welch's *t* test, $t = 2.832$, $p = 0.0135$) of NFH$^+$ axons compare to Gal3$^{+/+}$ lesion epicenters (Fig. 7*D*–*F*). These results further demonstrated a detrimental role for Gal3 during neurodegeneration.

Gal3 is increased during EAE and MS

Finally, we assessed Gal3 expression in EAE, an antigen driven model of MS and neuroinflammation (Glatigny and Bettelli, 2018). While Gal3 was absent in the contralateral NAWM of OxPC or LPC injected spinal cords (Figs. 2, 3), noninflamed (low accumulation of CD16/32$^+$ cells) NAWM of EAE spinal cords contained CD16/32$^-$ GFAP$^-$ Gal3$^+$ cells (Fig. 8*A*,*C*). Nevertheless, inflammatory EAE lesions highlighted by significant CD16/32$^+$ microglia/macrophage accumulation (Welch's *t* test, $t = 6.990$, $p = 0.0002$; Fig. 8*B*) had significantly elevated Gal3 immunoreactivity (Welch's *t* test, $t = 3.815$, $p = 0.0036$) compared with adjacent noninflamed NAWM (Fig. 8*C*). In addition, ~60% of CD16/32$^+$ cells in EAE lesions overlapped with Gal3$^+$ (Fig. 8*D*), suggesting microglia/macrophage increased Gal3 expression. Moreover, there was a significant increase of IBA1$^+$ microglia/macrophages (Welch's *t* test, $t = 3.757$, $p = 0.0183$) as well as a trend of increased Gal3 immunoreactivity (Welch's *t* test, $t = 2.387$, $p = 0.0682$) in EAE lesions from 52-week-old mice compared with lesions 8wk old mice (Extended Data Fig. 8-1), implicating Gal3 upregulation also associated with aging and greater immune cell accumulation during EAE.

Finally, to confirm whether Gal3 upregulation is relevant for CNS disease activity in humans, we measured its expression in MS. In tissue sections from three separate postmortem MS brains, there was greater Gal3 expression in lesion areas marked by increased accumulation of CD45$^+$ IBA1$^+$ ameboid leukocytes compared with the NAWM that mostly contained CD45$^+$

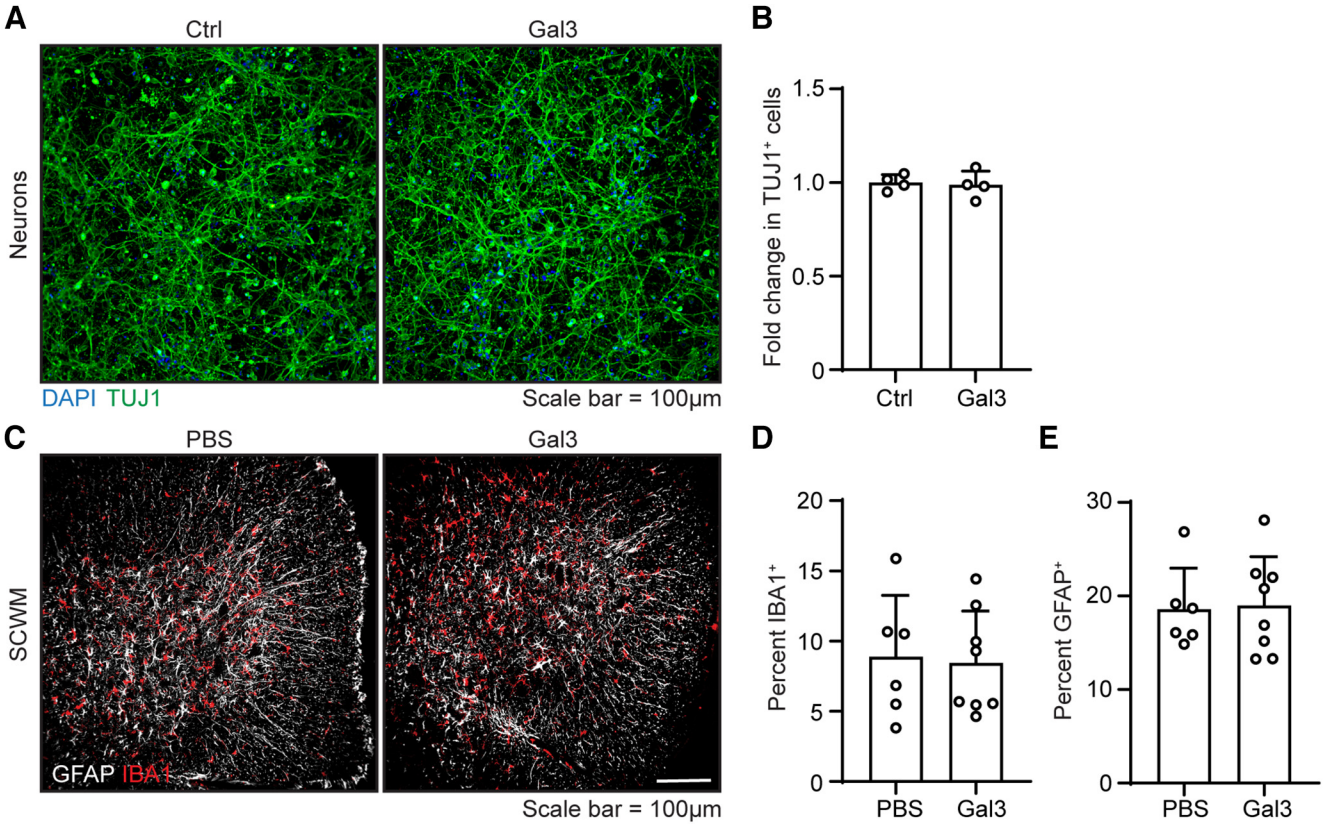

Figure 4. Gal3 alone is not neurotoxic. ***A***, Representative immunofluorescence images of primary mouse cortical neurons cultured in the presence or absence of 10 μg/ml of Gal3 for 24 h, labeled with DAPI (blue) and TUJ (TUJ1, green). ***B***, Representative graph comparing the fold difference in number of TUJ1$^+$ cells 24 h after control (Ctrl) or Gal3 treatment. Data shown four replicate samples, representative of two separate experiments, and shown as mean ± SD. Welch's unequal variances *t* test was used for statistical comparison. ***C***, Representative confocal images of SCWM from mice 3 d after PBS or mouse recombinant Gal3 injection, labeled with GFAP (gray), and IBA1 (red). ***D***, ***E***, Graphs comparing the percent IBA1$^+$ macrophages/microglia (***D***) and GFAP$^+$ astrocytes (***E***) in PBS and Gal3 injected SCWM. Data were acquired from two separate experiments, sample size $n = 4$ for PBS, $n = 8$ for Gal3, and represented as mean ± SD. Welch's unequal variances *t* test was used for statistical comparison.

IBA1$^+$ ramified microglia (Fig. 8*E–H*). Collectively, these observations indicate Gal3 upregulation and its association with microglia/macrophages are associated with aging and disease activity in the CNS.

Discussion

In this study, we show that Gal3 was upregulated and overexpressed in focal SCWM lesions of middle-aged mice, in EAE lesions, as well as in MS lesions. While Gal3 on its own did not cause damage to primary neurons or to the SCWM, the addition of excess Gal3 elevated IL-1β and exacerbated neurodegeneration in OxPC-induced SCWM lesions. OxPC are neurotoxic lipid peroxidation products found in MS lesions that require microglia-mediated clearance (Dong et al., 2021b). Unlike the addition of excess Gal3, OxPC-mediated damage was ameliorated in Gal3 deficient mice compared with normal mice. Collectively, our results suggest Gal3 overexpression by aging microglia may be a contributing factor to age-induced exacerbation of OxPC-mediated neurodegeneration (Dong et al., 2022).

Similar to our scRNAseq results that showed *Lgals3* overexpression by aging microglia during OxPC injury, recent studies also highlight *Lgal3* upregulation as a signature of aging and disease associated microglia (Krasemann et al., 2017; Hammond et al., 2019; Pluvinage et al., 2019; Plemel et al., 2020; Safaiyan et al., 2021; Boza-Serrano et al., 2022; Margeta et al., 2022). Interestingly, scRNAseq also showed BAM and monocyte/DC populations to express higher *Lgals3* than microglia from OxPC lesions and this is consistent with a recent study implicating Gal3 as a marker of peripheral derived cells in the CNS (Hohsfield et al., 2022). These cells may also be the same population of phagocytic Gal3$^+$ macrophages that associate with blood vessel injury in the brain (Mehina et al., 2021). However, since most immune cells accumulating in day 7 OxPC lesions are CNS resident microglia (Dong et al., 2021b, 2022), the *Lgals3^{hi}* BAM and monocyte/DC are unlikely the major Gal3 producers in aging OxPC lesions. Their *Lgals3* expression was also not impacted by age nor by OxPC, indicating they were not involved in the lesion response. However, these cells may be Gal3 reservoirs, and if they infiltrate into the CNS parenchyma because of blood brain barrier damage caused by EAE (Dias et al., 2021) or MS (Alvarez et al., 2011), they may release excess Gal3 into the lesion microenvironment. Indeed, while Gal3 was overexpressed in OxPC and lysolecithin focal SCWM lesions of 52-week-old middle-aged mice, there was minimal Gal3 in the lesions of six-week-old young mice. In contrast, there was abundant Gal3 immunoreactivity in EAE spinal cord lesions both 10- to 12-week-old young mice and 52-week-old middle-aged mice. Since monocytes and monocyte-derived cells are major drivers of EAE (Ajami et al., 2011; Yamasaki et al., 2014; Croxford et al., 2015), they are likely a major source of Gal3 which could contribute to disease pathology. Similarly, an increased number of monocyte and monocyte derived macrophages in the CNS because of advanced aging

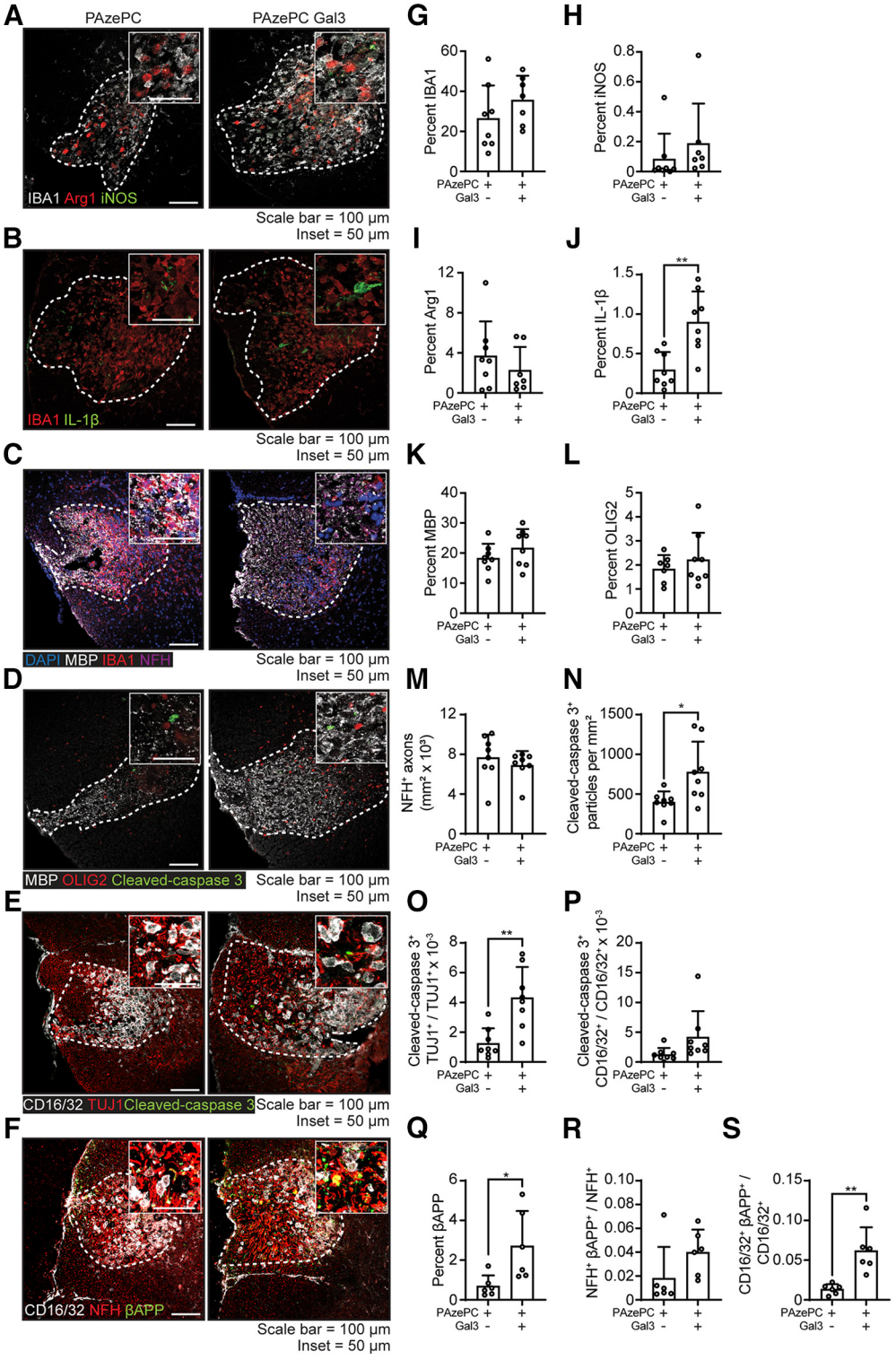

Figure 5. Gal3 elevates IL-1β, cleaved-caspase 3, and βAPP in OxPC lesions. ***A–F***, Representative confocal immunofluorescence images of day 3 SCWM lesions from PazePC alone or PazePC + Gal3 injected mice labeled with IBA1 (gray), Arg1 (red), and iNOS (green), or (***B***) with IBA1 (red) and IL-1β (green), or (***C***) with MBP (gray), IBA1 (red), and NFH (magenta) or (***D***) with MBP (gray), OLIG2 (red), and cleaved-caspase 3 (green), or (***E***) with CD16/32 (gray), TUJ1 (red), and cleaved-caspase 3 (green), or (***F***) with CD16/32 (gray), NFH (red), and βAPP (green). White dashed lines indicate the ROI used for quantitative analyses. ***G–S***, Graphs comparing IBA1 (***G***), iNOS (***H***), Arg1 (***I***), IL-1β (***J***), MBP (***K***), OLIG2 (***L***), NFH density (***M***), cleaved-caspase 3 particle density (***N***), proportion of cleaved-caspase 3 overlapping with TUJ1$^+$ axons (***O***) or with CD16/32$^+$ microglia/macrophages (***P***), βAPP (***Q***), as well as proportion of βAPP overlapping with NFH$^+$ axons (***R***) or with CD16/32$^+$ microglia/macrophages (***S***) between PAzePC alone or PAzePC + Gal3 lesions. Data were acquired from 2 separate experiments, sample size $n = 7$ or 8 per experimental group for all dataset, except in (***F***) and (***Q–S***) which had $n = 6$ per experimental group, and represented as mean ± SD. Significance indicated as $^*p < 0.05$, $^{**}p < 0.001$, Welch's unequal variances *t* test.

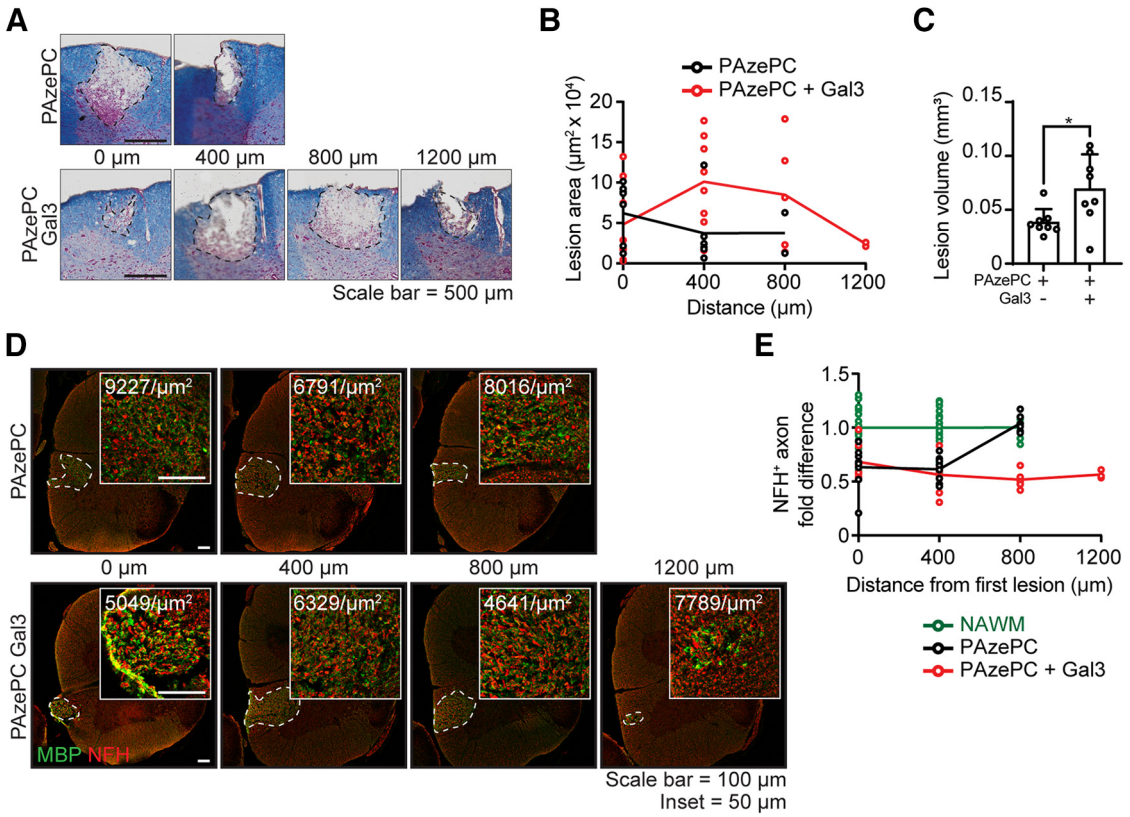

Figure 6. Gal3 increases OxPC-mediated neurodegeneration. ***A***, Representative EC and NR labeling of serial spinal cord sections from mice 3 d after PAzePC alone or PAzePC and Gal3 injection. Black dashed lines indicate the ROI used for quantitative analyses. ***B–C***) Graphs comparing day 3 spinal cord lesion spread (***B***) and total lesion volume (***C***) between PAzePC alone and PAzePC + Gal3 injected mice. ***D***, Representative confocal images of serial spinal cord sections from mice 3 d after PAzePC alone or PAzePC and Gal3 injection, labeled with MBP (gray) and NFH (red). Numbers in inset represent the number of NFH^+ axons per μm^2 within the lesion area. ***E***, Graph comparing fold difference of NFH^+ axon density in the PAzePC alone lesions or PAzePC and Gal3 lesions versus their respective contralateral NAWM, as a measure of the extent of overall axon loss. Data were acquired from two separate experiments, sample size $n = 8$ per experimental group, and represented as mean ± SD. Significance indicated as $^*p < 0.05$, Welch's unequal variances *t* test.

(Silvin et al., 2022) may produce Gal3 which inadvertently increase the susceptibility of the aging CNS to chronic neurodegeneration. Interestingly, some Gal3 immunoreactivity was also detected in $GFAP^-$ $CD16/32^-$ amoeboid cells in the EAE spinal cord. The identity of these cells and how they interact with $Gal3^+$ microglia/macrophages need additional study; but they may be neurons (Yoo et al., 2017) or even pericytes responding to injury (Özen et al., 2014). Whether Gal3 expression also exacerbates EAE pathology in the context of aging is an outstanding question and may be addressed by future studies comparing EAE in young and aging $Gal3^{+/+}$ and $Gal3^{-/-}$ mice. Finally, we provide new evidence of immune cell associated Gal3 within MS lesions, although our sample size was small and the data do not address different phases of MS disease progression. Thus, additional investigation is needed to clarify how the cell specificity and the spatiotemporal dynamics of Gal3 production by microglia, BAM, or monocytes and monocyte derived cells regulate neuroinflammation and neurodegeneration. These studies could lead to the identification of therapeutically targetable cell populations involved in MS progression or other neurodegenerative diseases.

The functional outcome of Gal3 deposition in the CNS during disease is not well understood. Gal3 may act as an endogenous TLR4 ligand for microglia (Burguillos et al., 2015) and this could explain why Gal3 deficiency attenuates neuroinflammation and neurodegeneration (Jiang et al., 2009; Margeta et al., 2022), as well as OxPC-mediated damage. However, direct injection of Gal3 into the SCWM did not promote astrocyte and microglia reactivity. This observation is more consistent with studies showing the ability of Gal3 to oligomerize and interact with lipopolysaccharide (LPS) to enhance inflammasome activation (Li et al., 2008; Fermino et al., 2011; Lo et al., 2021), rather than acting as a potent TLR4 ligand on its own. Since OxPC is also involved in TLR4 signaling (Di Gioia et al., 2020) and inflammasome activation (Yeon et al., 2017), Gal3 may amplify these signals in microglia from OxPC lesions. Although we did not specifically quantify cleaved IL-1β, the increased amount of total IL-1β and cleaved caspase 3 in OxPC lesions because of Gal3 addition resembles how Gal3 enhanced LPS-induced IL-1β production and caspase 4/11 activation (Lo et al., 2021). Interestingly, OxPC and Gal3 can both inhibit LPS-induced inflammation. OxPC compete with LPS for CD14 binding (Erridge et al., 2008), whereas Gal3 directly binds LPS (Li et al., 2008). Thus, additional studies are required to determine whether Gal3 directly interact with OxPC during injury and, if so, what are the signaling mechanisms involved.

Alternatively, Gal3 deposition in the CNS may act as a monocyte/macrophage chemoattractant (Sano et al., 2000). Indeed, Gal3 deficiency reduced immune cell infiltration into the CNS during EAE (Jiang et al., 2009) and Theiler's murine encephalomyelitis virus model of MS (James et al., 2016). Together with these studies, our results implicate Gal3 deposition in the CNS is detrimental, at least during the acute and inflammatory phases of disease. Given we show Gal3 accumulate with immune cells in MS lesions and other studies report its upregulation in neurologic conditions such as Alzheimer's disease (Boza-Serrano et al.,

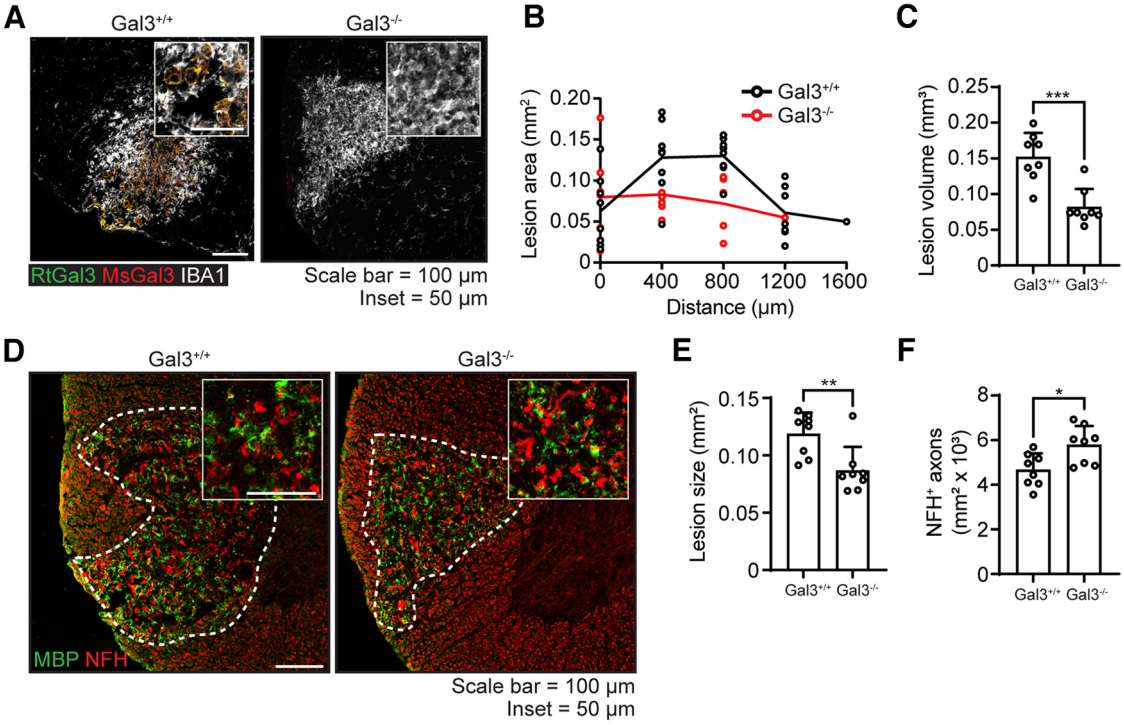

Figure 7. Gal3 deficiency reduces OxPC-mediated neurodegeneration. ***A***, Representative confocal immunofluorescence images of day 7 SCWM lesions from Gal3$^{+/+}$ or Gal3$^{-/-}$ mice injected with PazePC labeled with IBA1 (gray), mouse anti-Gal3 (red), and rat anti-Gal3 (green). ***B***, ***C***, Graphs comparing day 7 OxPC lesion spread (***B***) and total lesion volume (***C***) between Gal3$^{+/+}$ or Gal3$^{-/-}$ mice. ***D***, Representative confocal images of lesions from Gal3$^{+/+}$ or Gal3$^{-/-}$ mice labeled with NFH (red) and MBP (green). ***E***, ***F***, Graphs comparing day 7 OxPC lesion area (***E***) and lesional NFH^{+} axon density (***F***) between Gal3$^{+/+}$ or Gal3$^{-/-}$ mice. Data were acquired from two separate experiments, sample size $n = 8$ per experimental group, and represented as mean ± SD. Significance indicated as *$p < 0.05$, **$p < 0.01$, Welch's unequal variances *t* test.

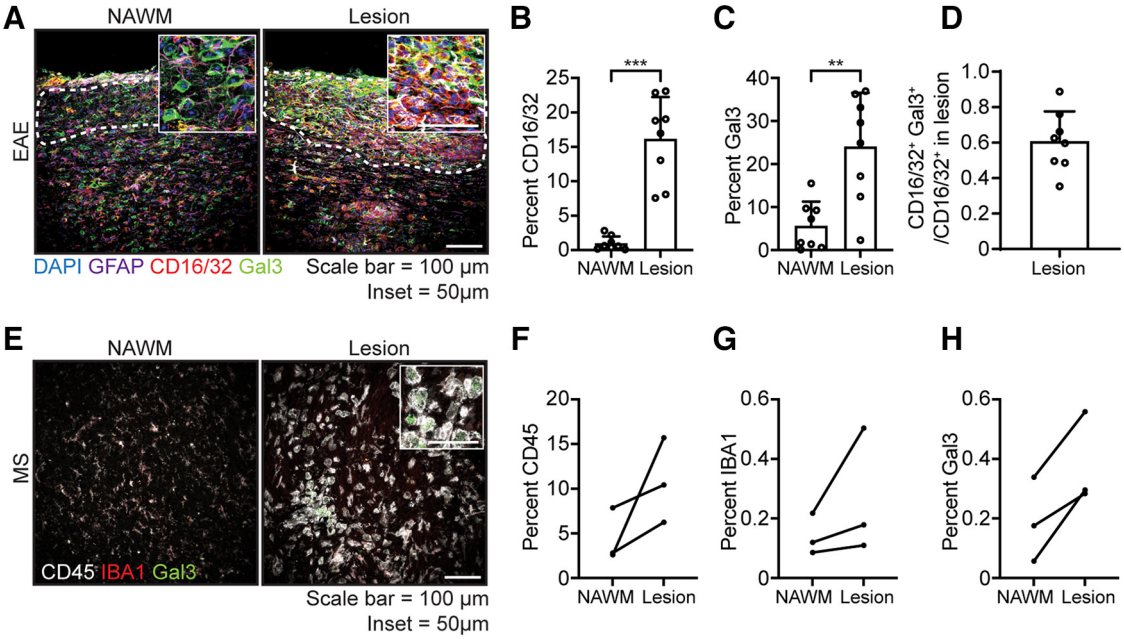

Figure 8. Gal3 is elevated in EAE and MS lesions. ***A***, Representative confocal images of inflamed EAE lesions or the noninflamed NAWM labeled with DAPI (blue), GFAP (magenta), Gal3 (green), and CD16/32 (red) 16–18 d after induction. White dashed lines indicate the ROI used for quantitative analyses. ***B–D***, Graph comparing the percent of lesion or NAWM ROI that is CD16/32^{+} (***B***), Gal3^{+} (***C***), and CD16/32^{+} Gal3^{+} over CD16/32^{+} proportions (***D***) in inflamed EAE lesions. Data were acquired from two separate experiments, sample size $n = 8$ per experimental group. ***E***, Representative confocal images of the lesion or the adjacent NAWM of postmortem MS brain sections labeled with CD45 (gray), IBA1 (red), and Gal3 (green). ***F–H***, Graph comparing the percent of lesion or NAWM ROI that is CD45^{+} (***F***), IBA1^{+} (***G***), and Gal3^{+} (***H***) in postmortem MS brain sections. Data were acquired from 3 different postmortem MS brains. Data are represented as mean ± SD for EAE data or as paired dots for MS data. Significance indicated as **$p < 0.01$, ***$p < 0.001$. Welch's unequal variances *t* test was used for ***B–D***. See Extended Data Figure 8-1.

2022), frontotemporal dementia (Huang et al., 2020), amyotrophic lateral sclerosis (Zhou et al., 2010) and glaucoma (Margeta et al., 2022), Gal3 may be an enticing therapeutic target. However, this requires additional careful investigation as Gal3 may also promote neuroprotective microglia/macrophage response during reparative phases of disease (Lalancette-Hébert et al., 2012; Quenum Zangbede et al., 2018).

In summary, we demonstrate elevated Gal3 deposition in OxPC and lysolecithin-induced focal SCWM lesions of aging mice, in EAE spinal cord lesions, and in MS brain lesions. Aging and disease associated Gal3 upregulation was closely associated with microglia/macrophages, but Gal3 on its own did not promote inflammation and injury in the CNS. However, excess Gal3 exacerbated OxPC-induced neurodegeneration and increased IL-1β levels in OxPC lesions whereas Gal3 deficiency ameliorated the damage. Thus, aging upregulated Gal3 may be involved in mechanisms that are detrimental to neurodegeneration and MS progression.

References

Ajami B, Bennett JL, Krieger C, McNagny KM, Rossi FM (2011) Infiltrating monocytes trigger EAE progression, but do not contribute to the resident microglia pool. Nat Neurosci 14:1142–1149.

Alvarez JI, Cayrol R, Prat A (2011) Disruption of central nervous system barriers in multiple sclerosis. Biochim Biophys Acta 1812:252–264.

Barake F, Soza A, González A (2020) Galectins in the brain: advances in neuroinflammation, neuroprotection and therapeutic opportunities. Curr Opin Neurol 33:381–390.

Bellver-Landete V, Bretheau F, Mailhot B, Vallières N, Lessard M, Janelle ME, Vernoux N, Tremblay ME, Fuehrmann T, Shoichet MS, Lacroix S (2019) Microglia are an essential component of the neuroprotective scar that forms after spinal cord injury. Nat Commun 10:518.

Boza-Serrano A, Vrillon A, Minta K, Paulus A, Camprubí-Ferrer L, Garcia M, Andreasson U, Antonell A, Wennström M, Gouras G, Dumurgier J, Cognat E, Molina-Porcel L, Balasa M, Vitorica J, Sánchez-Valle R, Paquet C, Venero JL, Blennow K, Deierborg T (2022) Galectin-3 is elevated in CSF and is associated with Abeta deposits and tau aggregates in brain tissue in Alzheimer's disease. Acta Neuropathol 144:843–859.

Burguillos MA, Svensson M, Schulte T, Boza-Serrano A, Garcia-Quintanilla A, Kavanagh E, Santiago M, Viceconte N, Oliva-Martin MJ, Osman AM, Salomonsson E, Amar L, Persson A, Blomgren K, Achour A, Englund E, Leffler H, Venero JL, Joseph B, Deierborg T (2015) Microglia-secreted galectin-3 acts as a toll-like receptor 4 ligand and contributes to microglial activation. Cell Rep 10:1626–1638.

Butler A, Hoffman P, Smibert P, Papalexi E, Satija R (2018) Integrating single-cell transcriptomic data across different conditions, technologies, and species. Nat Biotechnol 36:411–420.

Cantuti-Castelvetri L, Fitzner D, Bosch-Queralt M, Weil MT, Su M, Sen P, Ruhwedel T, Mitkovski M, Trendelenburg G, Lütjohann D, Möbius W, Simons M (2018) Defective cholesterol clearance limits remyelination in the aged central nervous system. Science 359:684–688.

Cignarella F, Filipello F, Bollman B, Cantoni C, Locca A, Mikesell R, Manis M, Ibrahim A, Deng L, Benitez BA, Cruchaga C, Licastro D, Mihindukulasuriya K, Harari O, Buckland M, Holtzman DM, Rosenthal A, Schwabe T, Tassi I, Piccio L (2020) TREM2 activation on microglia promotes myelin debris clearance and remyelination in a model of multiple sclerosis. Acta Neuropathol 140:513–534.

Croxford AL, Lanzinger M, Hartmann FJ, Schreiner B, Mair F, Pelczar P, Clausen BE, Jung S, Greter M, Becher B (2015) The cytokine GM-CSF drives the inflammatory signature of CCR2+ monocytes and licenses autoimmunity. Immunity 43:502–514.

Cua RC, Lau LW, Keough MB, Midha R, Apte SS, Yong VW (2013) Overcoming neurite-inhibitory chondroitin sulfate proteoglycans in the astrocyte matrix. Glia 61:972–984.

Damani MR, Zhao L, Fontainhas AM, Amaral J, Fariss RN, Wong WT (2011) Age-related alterations in the dynamic behavior of microglia. Aging Cell 10:263–276.

Davalos D, Grutzendler J, Yang G, Kim JV, Zuo Y, Jung S, Littman DR, Dustin ML, Gan WB (2005) ATP mediates rapid microglial response to local brain injury in vivo. Nat Neurosci 8:752–758.

Dias DO, Kalkitsas J, Kelahmetoglu Y, Estrada CP, Tatarishvili J, Holl D, Jansson L, Banitalebi S, Amiry-Moghaddam M, Ernst A, Huttner HB, Kokaia Z, Lindvall O, Brundin L, Frisén J, Göritz C (2021) Pericyte-derived fibrotic scarring is conserved across diverse central nervous system lesions. Nat Commun 12:5501.

Diaz-Aparicio I, Paris I, Sierra-Torre V, Plaza-Zabala A, Rodríguez-Iglesias N, Márquez-Ropero M, Beccari S, Huguet P, Abiega O, Alberdi E, Matute C, Bernales I, Schulz A, Otrokocsi L, Sperlagh B, Happonen KE, Lemke G, Maletic-Savatic M, Valero J, Sierra A (2020) Microglia actively remodel adult hippocampal neurogenesis through the phagocytosis secretome. J Neurosci 40:1453–1482.

Di Gioia M, Spreafico R, Springstead JR, Mendelson MM, Joehanes R, Levy D, Zanoni I (2020) Endogenous oxidized phospholipids reprogram cellular metabolism and boost hyperinflammation. Nat Immunol 21:42–53.

Dong Y, Yong VW (2019) When encephalitogenic T cells collaborate with microglia in multiple sclerosis. Nat Rev Neurol 15:704–717.

Dong Y, Yong VW (2022) Oxidized phospholipids as novel mediators of neurodegeneration. Trends Neurosci 45:419–429.

Dong Y, Lozinski BM, Silva C, Yong VW (2021a) Studying the microglia response to oxidized phosphatidylcholine in primary mouse neuron culture and mouse spinal cord. STAR Protoc 2:100853.

Dong Y, D'Mello C, Pinsky W, Lozinski BM, Kaushik DK, Ghorbani S, Moezzi D, Brown D, Melo FC, Zandee S, Vo T, Prat A, Whitehead SN, Yong VW (2021b) Oxidized phosphatidylcholines found in multiple sclerosis lesions mediate neurodegeneration and are neutralized by microglia. Nat Neurosci 24:489–503.

Dong Y, Jain RW, Lozinski BM, D'Mello C, Visser F, Ghorbani S, Zandee S, Brown DI, Prat A, Xue M, Yong VW (2022) Single-cell and spatial RNA sequencing identify perturbators of microglial functions with aging. Nat Aging 2:508–525.

Ennerfelt H, Frost EL, Shapiro DA, Holliday C, Zengeler KE, Voithofer G, Bolte AC, Lammert CR, Kulas JA, Ulland TK, Lukens JR (2022) SYK coordinates neuroprotective microglial responses in neurodegenerative disease. Cell 185:4135–4152.e22.

Erridge C, Kennedy S, Spickett CM, Webb DJ (2008) Oxidized phospholipid inhibition of Toll-like receptor (TLR) signaling is restricted to TLR2 and TLR4 - roles for CD14, LPS-binding protein, and MD2 as targets for specificity of inhibition. J Biol Chem 283:24748–24759.

Fermino ML, Polli CD, Toledo KA, Liu FT, Hsu DK, Roque-Barreira MC, Pereira-da-Silva G, Bernardes ES, Halbwachs-Mecarelli L (2011) LPS-induced galectin-3 oligomerization results in enhancement of neutrophil activation. PLoS One 6:e26004.

Glatigny S, Bettelli E (2018) Experimental autoimmune encephalomyelitis (EAE) as animal models of multiple sclerosis (MS). Cold Spring Harb Perspect Med 8:a028977.

Haider L, Fischer MT, Frischer JM, Bauer J, Höftberger R, Botond G, Esterbauer H, Binder CJ, Witztum JL, Lassmann H (2011) Oxidative damage in multiple sclerosis lesions. Brain 134:1914–1924.

Hammond TR, Dufort C, Dissing-Olesen L, Giera S, Young A, Wysoker A, Walker AJ, Gergits F, Segel M, Nemesh J, Marsh SE, Saunders A, Macosko E, Ginhoux F, Chen J, Franklin RJM, Piao X, McCarroll SA, Stevens B (2019) Single-cell RNA sequencing of microglia throughout the mouse lifespan and in the injured brain reveals complex cell-state changes. Immunity 50:253–271.e6.

Hefendehl JK, Neher JJ, Sühs RB, Kohsaka S, Skodras A, Jucker M (2014) Homeostatic and injury-induced microglia behavior in the aging brain. Aging Cell 13:60–69.

Herzog C, Pons Garcia L, Keatinge M, Greenald D, Moritz C, Peri F, Herrgen L (2019) Rapid clearance of cellular debris by microglia limits secondary neuronal cell death after brain injury in vivo. Development 146:dev174698.

Hohsfield LA, Tsourmas KI, Ghorbanian Y, Syage AR, Kim SJ, Cheng YT, Furman S, Inlay MA, Lane TE, Green KN (2022) MAC2 is a long-lasting marker of peripheral cell infiltrates into the mouse CNS after bone marrow transplantation and coronavirus infection. Glia 70:875–891.

Hou Y, Dan X, Babbar M, Wei Y, Hasselbalch SG, Croteau DL, Bohr VA (2019) Ageing as a risk factor for neurodegenerative disease. Nat Rev Neurol 15:565–581.

Huang M, Modeste E, Dammer E, Merino P, Taylor G, Duong DM, Deng Q, Holler CJ, Gearing M, Dickson D, Seyfried NT, Kukar T (2020) Network analysis of the progranulin-deficient mouse brain proteome reveals pathogenic mechanisms shared in human frontotemporal dementia caused by GRN mutations. Acta Neuropathol Commun 8:163.

Jäckle K, Zeis T, Schaeren-Wiemers N, Junker A, van der Meer F, Kramann N, Stadelmann C, Brück W (2020) Molecular signature of slowly expanding lesions in progressive multiple sclerosis. Brain 143:2073–2088.

James RE, Hillis J, Adorján I, Gration B, Mundim MV, Iqbal AJ, Majumdar MM, Yates RL, Richards MM, Goings GE, DeLuca GC, Greaves DR, Miller SD, Szele FG (2016) Loss of galectin-3 decreases the number of immune cells in the subventricular zone and restores proliferation in a viral model of multiple sclerosis. Glia 64:105–121.

Jiang HR, Al Rasebi Z, Mensah-Brown E, Shahin A, Xu D, Goodyear CS, Fukada SY, Liu FT, Liew FY, Lukic ML (2009) Galectin-3 deficiency reduces the severity of experimental autoimmune encephalomyelitis. J Immunol 182:1167–1173.

Kaya T, Mattugini N, Liu L, Ji H, Cantuti-Castelvetri L, Wu J, Schifferer M, Groh J, Martini R, Besson-Girard S, Kaji S, Liesz A, Gokce O, Simons M (2022) CD8(+) T cells induce interferon-responsive oligodendrocytes and microglia in white matter aging. Nat Neurosci 25:1446–1457.

Keren-Shaul H, Spinrad A, Weiner A, Matcovitch-Natan O, Dvir-Szternfeld R, Ulland TK, David E, Baruch K, Lara-Astaiso D, Toth B, Itzkovitz S, Colonna M, Schwartz M, Amit I (2017) A unique microglia type associated with restricting development of Alzheimer's disease. Cell 169:1276–1290.e17.

Krasemann S, et al. (2017) The TREM2-APOE pathway drives the transcriptional phenotype of dysfunctional microglia in neurodegenerative diseases. Immunity 47:566–581.e9.

Lalancette-Hébert M, Swarup V, Beaulieu JM, Bohacek I, Abdelhamid E, Weng YC, Sato S, Kriz J (2012) Galectin-3 is required for resident microglia activation and proliferation in response to ischemic injury. J Neurosci 32:10383–10395.

Lampron A, Larochelle A, Laflamme N, Préfontaine P, Plante MM, Sánchez MG, Yong VW, Stys PK, Tremblay ME, Rivest S (2015) Inefficient clearance of myelin debris by microglia impairs remyelinating processes. J Exp Med 212:481–495.

Li Y, Komai-Koma M, Gilchrist DS, Hsu DK, Liu FT, Springall T, Xu D (2008) Galectin-3 is a negative regulator of lipopolysaccharide-mediated inflammation. J Immunol 181:2781–2789.

Lo TH, Chen HL, Yao CI, Weng IC, Li CS, Huang CC, Chen NJ, Lin CH, Liu FT (2021) Galectin-3 promotes noncanonical inflammasome activation through intracellular binding to lipopolysaccharide glycans. Proc Natl Acad Sci U S A 118:e2026246118.

Madry C, Kyrargyri V, Arancibia-Cárcamo IL, Jolivet R, Kohsaka S, Bryan RM, Attwell D (2018) Microglial ramification, surveillance, and interleukin-1β release are regulated by the two-pore domain K(+) channel THIK-1. Neuron 97:299–312.e6.

Mandrekar S, Jiang Q, Lee CY, Koenigsknecht-Talboo J, Holtzman DM, Landreth GE (2009) Microglia mediate the clearance of soluble Abeta through fluid phase macropinocytosis. J Neurosci 29:4252–4262.

Margeta MA, Yin Z, Madore C, Pitts KM, Letcher SM, Tang J, Jiang S, Gauthier CD, Silveira SR, Schroeder CM, Lad EM, Proia AD, Tanzi RE, Holtzman DM, Krasemann S, Chen DF, Butovsky O (2022) Apolipoprotein E4 impairs the response of neurodegenerative retinal microglia and prevents neuronal loss in glaucoma. Immunity 55:1627–1644.e7.

Mehina EMF, Taylor S, Boghozian R, White E, Choi SE, Cheema MS, Korbelin J, Brown CE (2021) Invasion of phagocytic galectin 3 expressing macrophages in the diabetic brain disrupts vascular repair. Sci Adv 7:eabg2712.

Michaels NJ, Lemmon K, Plemel JR, Jensen SK, Mishra MK, Brown D, Rawji KS, Koch M, Yong VW (2020) Aging-exacerbated acute axon and myelin injury is associated with microglia-derived reactive oxygen species and is alleviated by the generic medication indapamide. J Neurosci 40:8587–8600.

Muñoz U, Sebal C, Escudero E, Esiri M, Tzartos J, Sloan C, Sadaba MC (2022) Main role of antibodies in demyelination and axonal damage in multiple sclerosis. Cell Mol Neurobiol 42:1809–1827.

Namura S, Zhu J, Fink K, Endres M, Srinivasan A, Tomaselli KJ, Yuan J, Moskowitz MA (1998) Activation and cleavage of caspase-3 in apoptosis induced by experimental cerebral ischemia. J Neurosci 18:3659–3668.

Olah M, et al. (2020) Single cell RNA sequencing of human microglia uncovers a subset associated with Alzheimer's disease. Nat Commun 11:6129.

Özen I, Deierborg T, Miharada K, Padel T, Englund E, Genové G, Paul G (2014) Brain pericytes acquire a microglial phenotype after stroke. Acta Neuropathol 128:381–396.

Parkhurst CN, Yang G, Ninan I, Savas JN, Yates JR 3rd, Lafaille JJ, Hempstead BL, Littman DR, Gan WB (2013) Microglia promote learning-dependent synapse formation through brain-derived neurotrophic factor. Cell 155:1596–1609.

Plemel JR, Michaels NJ, Weishaupt N, Caprariello AV, Keough MB, Rogers JA, Yukseloglu A, Lim J, Patel VV, Rawji KS, Jensen SK, Teo W, Heyne B, Whitehead SN, Stys PK, Yong VW (2018) Mechanisms of lysophosphatidylcholine-induced demyelination: a primary lipid disrupting myelinopathy. Glia 66:327–347.

Plemel JR, et al. (2020) Microglia response following acute demyelination is heterogeneous and limits infiltrating macrophage dispersion. Sci Adv 6:eaay6324.

Pluvinage JV, Haney MS, Smith BAH, Sun J, Iram T, Bonanno L, Li L, Lee DP, Morgens DW, Yang AC, Shuken SR, Gate D, Scott M, Khatri P, Luo J, Bertozzi CR, Bassik MC, Wyss-Coray T (2019) CD22 blockade restores homeostatic microglial phagocytosis in ageing brains. Nature 568:187–192.

Puigdellívol M, Allendorf DH, Brown GC (2020) Sialylation and galectin-3 in microglia-mediated neuroinflammation and neurodegeneration. Front Cell Neurosci 14:162.

Quenum Zangbede FO, Chauhan A, Sharma J, Mishra BB (2018) Galectin-3 in M2 macrophages plays a protective role in resolution of neuropathology in brain parasitic infection by regulating neutrophil turnover. J Neurosci 38:6737–6750.

Rawji KS, Kappen J, Tang WW, Teo WL, Plemel JR, Stys PK, Yong VW (2018) Deficient surveillance and phagocytic activity of myeloid cells within demyelinated lesions in aging mice visualized by ex vivo live multiphoton imaging. J Neurosci 38:1973–1988.

Safaiyan S, Besson-Girard S, Kaya T, Cantuti-Castelvetri L, Liu L, Ji H, Schifferer M, Gouna G, Usifo F, Kannaiyan N, Fitzner D, Xiang X, Rossner MJ, Brendel M, Gokce O, Simons M (2021) White matter aging drives microglial diversity. Neuron 109:1100–1117.e10.

Sano H, Hsu DK, Yu L, Apgar JR, Kuwabara I, Yamanaka T, Hirashima M, Liu FT (2000) Human galectin-3 is a novel chemoattractant for monocytes and macrophages. J Immunol 165:2156–2164.

Silvin A, et al. (2022) Dual ontogeny of disease-associated microglia and disease inflammatory macrophages in aging and neurodegeneration. Immunity 55:1448–1465.e6.

Tan Y, Zheng Y, Xu D, Sun Z, Yang H, Yin Q (2021) Galectin-3: a key player in microglia-mediated neuroinflammation and Alzheimer's disease. Cell Biosci 11:78.

von Leden RE, Khayrullina G, Moritz KE, Byrnes KR (2017) Age exacerbates microglial activation, oxidative stress, inflammatory and NOX2 gene expression, and delays functional recovery in a middle-aged rodent model of spinal cord injury. J Neuroinflammation 14:161.

Willis EF, MacDonald KPA, Nguyen QH, Garrido AL, Gillespie ER, Harley SBR, Bartlett PF, Schroder WA, Yates AG, Anthony DC, Rose-John S, Ruitenberg MJ, Vukovic J (2020) Repopulating microglia promote brain repair in an IL-6-dependent manner. Cell 180:833–846.e16.

Yamasaki R, et al. (2014) Differential roles of microglia and monocytes in the inflamed central nervous system. J Exp Med 211:1533–1549.

Yeon SH, Yang G, Lee HE, Lee JY (2017) Oxidized phosphatidylcholine induces the activation of NLRP3 inflammasome in macrophages. J Leukoc Biol 101:205–215.

Yong HYF, Yong VW (2022) Mechanism-based criteria to improve therapeutic outcomes in progressive multiple sclerosis. Nat Rev Neurol 18:40–55.

Yoo HI, Kim EG, Lee EJ, Hong SY, Yoon CS, Hong MJ, Park SJ, Woo RS, Baik TK, Song DY (2017) Neuroanatomical distribution of galectin-3 in the adult rat brain. J Mol Histol 48:133–146.

Zhou JY, Afjehi-Sadat L, Asress S, Duong DM, Cudkowicz M, Glass JD, Peng J (2010) Galectin-3 is a candidate biomarker for amyotrophic lateral sclerosis: discovery by a proteomics approach. J Proteome Res 9:5133–5141.

Zrzavy T, Hametner S, Wimmer I, Butovsky O, Weiner HL, Lassmann H (2017) Loss of 'homeostatic' microglia and patterns of their activation in active multiple sclerosis. Brain 140:1900–1913.

Zrzavy T, Schwaiger C, Wimmer I, Berger T, Bauer J, Butovsky O, Schwab JM, Lassmann H, Höftberger R (2021) Acute and non-resolving inflammation associate with oxidative injury after human spinal cord injury. Brain 144:144–161.